(4)

TECHNICAL REPORT NO. 16

To

The Office of Naval Research
Contract No. N00014-86-K-0381

ADVANCED PROCESSING AND PROPERTIES OF HIGH PERFORMANCE ALLOYS

D. A. Koss

Department of Materials Science and Engineering
The Pennsylvania State University
University Park, PA 16802

Report for the period 1 January 1989 - December 31, 1989

SECURITY CLASSIFICATION OF THIS PAGE

REPORT DOCUMENTATION PAGE

Form Approved
OMB No. 0704-0188

1a REPORT SECURITY CLASSIFICATION: Technical Report No. 16

1b RESTRICTIVE MARKINGS: unclassified

2a SECURITY CLASSIFICATION AUTHORITY:

2b DECLASSIFICATION / DOWNGRADING SCHEDULE:

3 DISTRIBUTION / AVAILABILITY OF REPORT: unlimited

4 PERFORMING ORGANIZATION REPORT NUMBER(S):

5 MONITORING ORGANIZATION REPORT NUMBER(S):

6a NAME OF PERFORMING ORGANIZATION: The Pennsylvania State Univ.

6b OFFICE SYMBOL (If applicable):

7a NAME OF MONITORING ORGANIZATION:

6c. ADDRESS (City, State, and ZIP Code):
Department of Materials Science & Engineering
University Park, PA 16802

7b ADDRESS (City, State, and ZIP Code):

8a. NAME OF FUNDING / SPONSORING ORGANIZATION: Office of Naval Research

8b OFFICE SYMBOL (If applicable):

9 PROCUREMENT INSTRUMENT IDENTIFICATION NUMBER:

8c. ADDRESS (City, State, and ZIP Code):
800 N. Quincy St.
Arlington, VA 22217

10 SOURCE OF FUNDING NUMBERS

PROGRAM ELEMENT NO	PROJECT NO	TASK NO	WORK UNIT ACCESSION NO

11 TITLE (Include Security Classification): Advanced Processing and Properties of High Performance Alloys

12 PERSONAL AUTHOR(S): D. A. Koss

13a. TYPE OF REPORT	13b TIME COVERED	14 DATE OF REPORT (Year, Month, Day)	15 PAGE COUNT
	FROM 1/1/89 TO 12/31/89	April 1990	21

16 SUPPLEMENTARY NOTATION:

17 COSATI CODES

FIELD	GROUP	SUB-GROUP

18 SUBJECT TERMS (Continue on reverse if necessary and identify by block number):
Metal[illegible], [illegible]um, Alloys, Strength [illegible], Mechanical Properties, Fracture Mechanics, Mater[illegible]

19 ABSTRACT (Continue on reverse if necessary and identify by block number)

Progress is reviewed for a research program whose purpose is to establish a broad-based understanding of the application and consequences of advanced processing techniques, especially as they influence the strength and fracture resistance of high performance structural alloys. While some of the research is specific to certain alloy systems, much of the program constitutes fundamental study of the deformation and fracture of engineering alloys containing processing-induced defects. Progress for the period January 1, 1989, to December 31, 1989, is reviewed for the following projects within the program:
(1) modeling the effects of pores or voids on fracture,
(2) the processing and properties of Cu-Nb alloy, and
(3) a new age-hardenable beta titanium system.

20 DISTRIBUTION / AVAILABILITY OF ABSTRACT: ☐ UNCLASSIFIED/UNLIMITED ☒ SAME AS RPT ☐ DTIC USERS

21 ABSTRACT SECURITY CLASSIFICATION:

22a NAME OF RESPONSIBLE INDIVIDUAL: D. A. Koss

22b TELEPHONE (Include Area Code): 814-865-5447

22c OFFICE SYMBOL:

DD Form 1473, JUN 86 — Previous editions are obsolete — SECURITY CLASSIFICATION OF THIS PAGE

S/N 0102-LF-014-6603

ADVANCED PROCESSING AND PROPERTIES OF HIGH PERFORMANCE ALLOYS

Introduction

The performance of advanced structural systems is becoming increasingly limited by alloys which must demonstrate improved strength, fracture resistance, and reliability. The continued development of such alloys depends increasingly on advanced and often innovative processing techniques. However, this creates problems. For example, such processing often results in residual defects, such as porosity, which control the fracture resistance of the material. Furthermore, the rate of application of new processing methods is exceeding the knowledge base necessary to predict the associated microstructures and resulting behavior of the component in service. Thus there is a critical need not only to predict the microstructural evolution as a result of advanced processing techniques but also to develop computational models which predict fracture behavior and cracking resistance of the resulting high performance materials.

The primary purpose of the present research is to provide a broad-based understanding of the applications and consequences, particularly as regard the fracture behavior, of certain advanced processing techniques used to obtain new high performance alloys. The research has ranged from computational modeling studies of the effects of void or pores on both monotonic and cyclic fracture to the application of advanced gas atomization to obtain unique microstructures and improved mechanical properties in certain alloy systems, such as Cu-Nb. The present report summarizes research for the period 1/1/89 to 12/31/89 performed under the auspices of Contract No. N00014-86-K-0381. The research areas are as follows:

1) computational modeling of void/pore effects on fracture,
2) the application of high pressure gas atomization to alloys susceptible to liquid phase separation, and
3) a new age-hardenable beta titanium alloy.

A significant aspect of the research program is the educational experience provided to the graduate students involved. The following students have been a part of this ONR Program during 1989:

Kevin Zeik, Ph.D, candidate,

Andrew Geltmacher, M. S. candidate, and

Louis Quattrocchi, M.S. candidate.

Summary of Research

1 MODELING THE EFFECTS OF PORES OR VOIDS ON FRACTURE [with A. Geltmacher, M. S. candidate, and D. Gerard, Ph.D].

(a) Pore-shape Effects on Tensile Fracture

The effect of porosity or voids on the ductility of porous metals is well known; see ref. 1 for review. In particular, it has been established experimentally that metals containing rounded porosity are more ductile than those containing irregularly-shaped pores at the same volume fraction of porosity [2]. Pore-shape effects have been analyzed on a qualitative basis in terms of plastic strain distribution differences between rounded and angular porosity [2] and on a quantitative basis with regard to the effect of pore geometry on tensile strength, but not ductility [3]. The latter analysis is restricted by its reliance on regular arrays of holes [4], while the former offers no quantitative insight. Thus, comparatively little is known of the mechanism(s) responsible for pore-shape effects on fracture, especially with reference to the implications of such mechanisms. The purpose of this study is to model the effect of pore shapes on the ductile fracture of porous metals. Particular attention in this initial effort is being given to the influence of the spatial distribution of the pores, the strain-hardening behavior of the matrix, and the role of the volume fraction of porosity on pore-shape effects.

The present study utilizes a computer model which simulates three-dimensional pore distributions by two-dimensional arrays of through-thickness equisized holes in sheet specimens wherein deformation occurs primarily under plane-stress conditions [4-7]. Fig. 1 shows an example of such a hole array. Two-dimensional modeling of the fracture of porous or voided

metals using arrays of holes has been performed several times in the past, although almost always on the basis of regular arrays. As may be recognized in Fig. 1, a principal advantage of the present modeling approach is the ability to simulate the random nature of the spatial distributions(s) of pores in real metals. Our simulation is clearly a very simplified version of the realistic case in which pores or voids of various shapes and sizes exist in three-dimensional space and wherein failure of the specimen is associated with either flow localization or cracking causing linking between pores. Difficulties in determining three-dimensional strain distributions and pore-linking criteria among random distributions of pores preclude a rigorous three-dimensional simulation. However, the methodology and significant trends predicted by the present two-dimensional analysis are consistent with both plane-stress and plane-strain experiments [4-7] and should be valid for a three-dimensional porous metal. This initial analysis assumes void/pore linking due to flow instability between pores or voids.

The present analysis is based on the utilization of a computer simulation [6,7] which predicts the ductility behavior of specimens that possess pseudo- random arrays of through-thickness holes, which are subject to a minimum interhole spacing within which adjacent holes cannot exist. In the present study, the simulation is extended to contrast the behavior of specimens containing elongated vs. circular holes. Fig. 2 shows the two hole geometries used in the simulations. The elongated hole has a length to width ratio of 4/1, and the major axes of the elongated holes are maintained perpendicular to the tensile direction, since the strain localization effect of the elongated holes is maximized under this condition. The dimensions of the circular and elongated holes were selected such that the areas of the holes are a constant value. In the computer simulation, the strain fields of the elongated holes are obtained from empirical relations based on experiments utilizing pairs of circular holes in either 1000 Al or alpha brass which have been linked by a free surface prior to deformation [6,7]. Hole linking is assumed to occur at a critical value of the thickness strain [6]. Other pertinent details are described elsewhere [8].

The effect of hole shape on the ductility is shown in Fig's. 3 and 4 for '1100 aluminum' and '70-30 brass', respectively. An examination of Fig's 3 and 4 indicates the following trends:

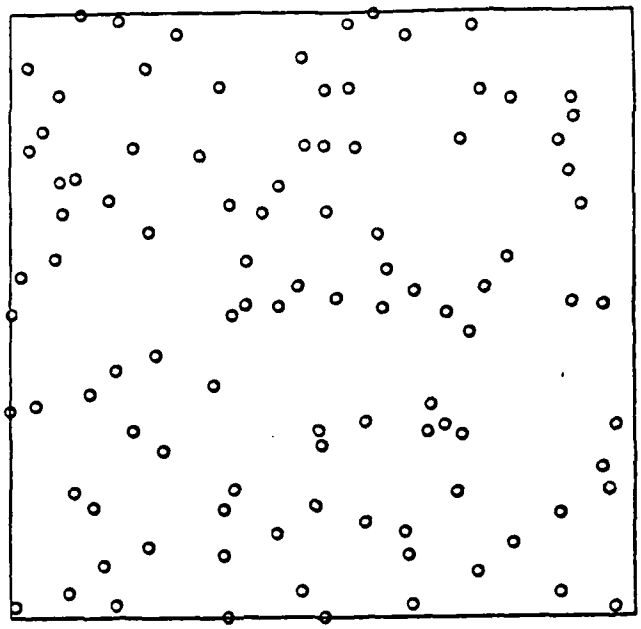

Figure 1. An example of an "inhibited" random hole array containing .02 area fraction of 2.916mm diameter circular holes, with an interhole spacing of 1.0mm.

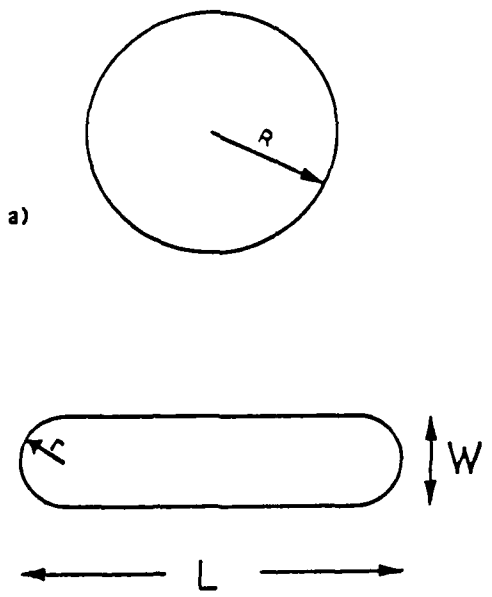

Figure 2. Hole geometries used in this study: (a) circular (R=1.098mm) and (b) elongated (r=0.5mm and the length to width ratio of 4 to 1).

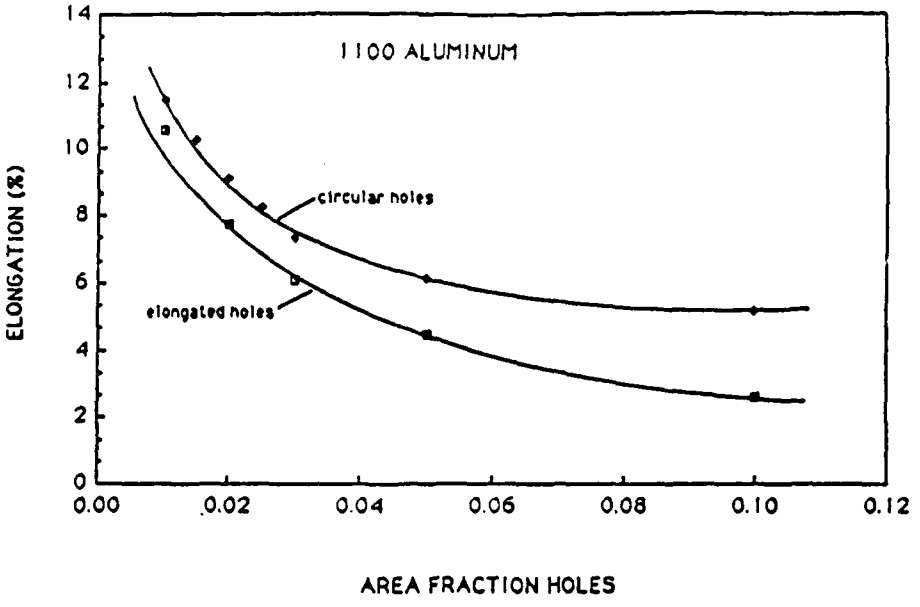

Figure 3. The predicted dependence of elongation to failure on area fraction for both circular and elongated holes for a material whose strain hardening corresponds to annealed 1100 Al.

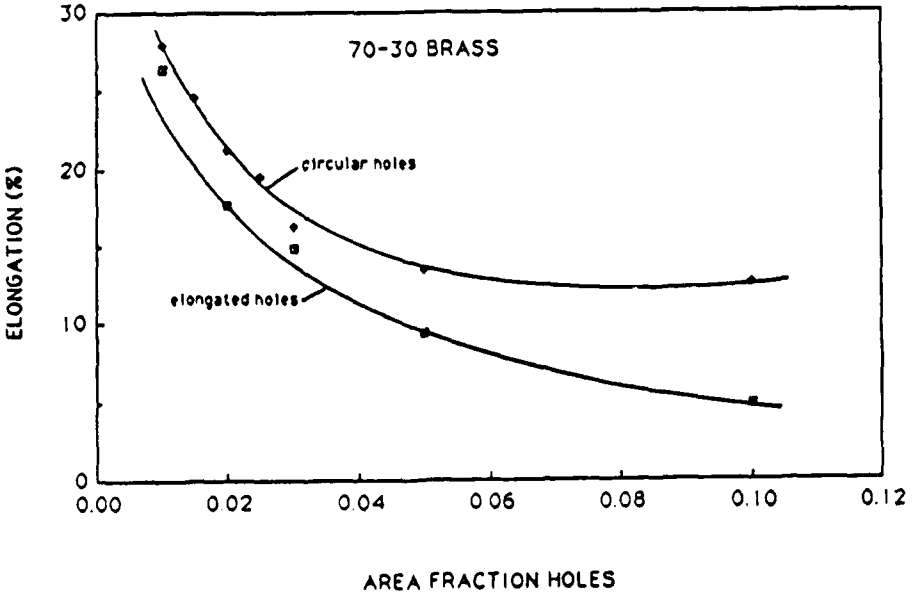

Figure 4. The predicted dependence of elongation to failure on area fraction for both circular and elongated holes for a material whose strain hardening corresponds to annealed alpha brass.

(1) The ductility decreases as the area fraction of holes increases for both circular and elongated holes. This may be understood on the basis of strain localization near holes (or pores). Thus, the critical strain for hole linking which is achieved at smaller macroscopic strains when adjacent holes are spaced closely together; this is a result of the increased overlap of strain fields at small hole spacings. Thus, hole/pore linking occurs more readily at high hole/pore contents due to decreased interhole/pore spacings.

(2) Comparing Fig's. 3 and 4 indicates that the predicted ductility of the brass specimens is greater than that of the 1100 Al. This suggest that strain-induced pore linking is easier in materials with low strain hardening capacity. The cause for this behavior is evident in comparison of the magnitude of the local strains which develop near holes in the 'Al' compared to the 'brass' at the same macroscopic strain level. For example, comparing Fig. 5a to Fig. 5b indicates that at a macroscopic strain of 0.10, the local strains near the holes in the 'Al' are nearly four times greater than those in the 'brass'. Thus very high local strain levels are created near the holes in the 'low-hardening' Al, while the high n-value of brass diffuses the strain effectively. As a result, hole linking by either crack initiation or flow localization, is expected to occur at smaller macroscopic strain levels in the 'Al', decreasing its ductility to less than that of the 'brass'.

(3) Ductility of specimens with elongated holes is less than that of specimens with circular holes. Fig. 5 shows that elongated holes act to increase dramatically the level of local strain adjacent to a hole. Thus, the critical local strain to initiate a crack or cause flow localization is achieved at a smaller applied macroscopic strain if the holes are elongated. This results in accelerated hole linking and therefore decreased ductility.

(4) The hole-shape effect depends on the area fraction of holes being largest at high area fractions of holes. Although somewhat surprising, this prediction is quite reasonable in view of Fig. 5, if pore linking occurs by a localized flow instability process and not

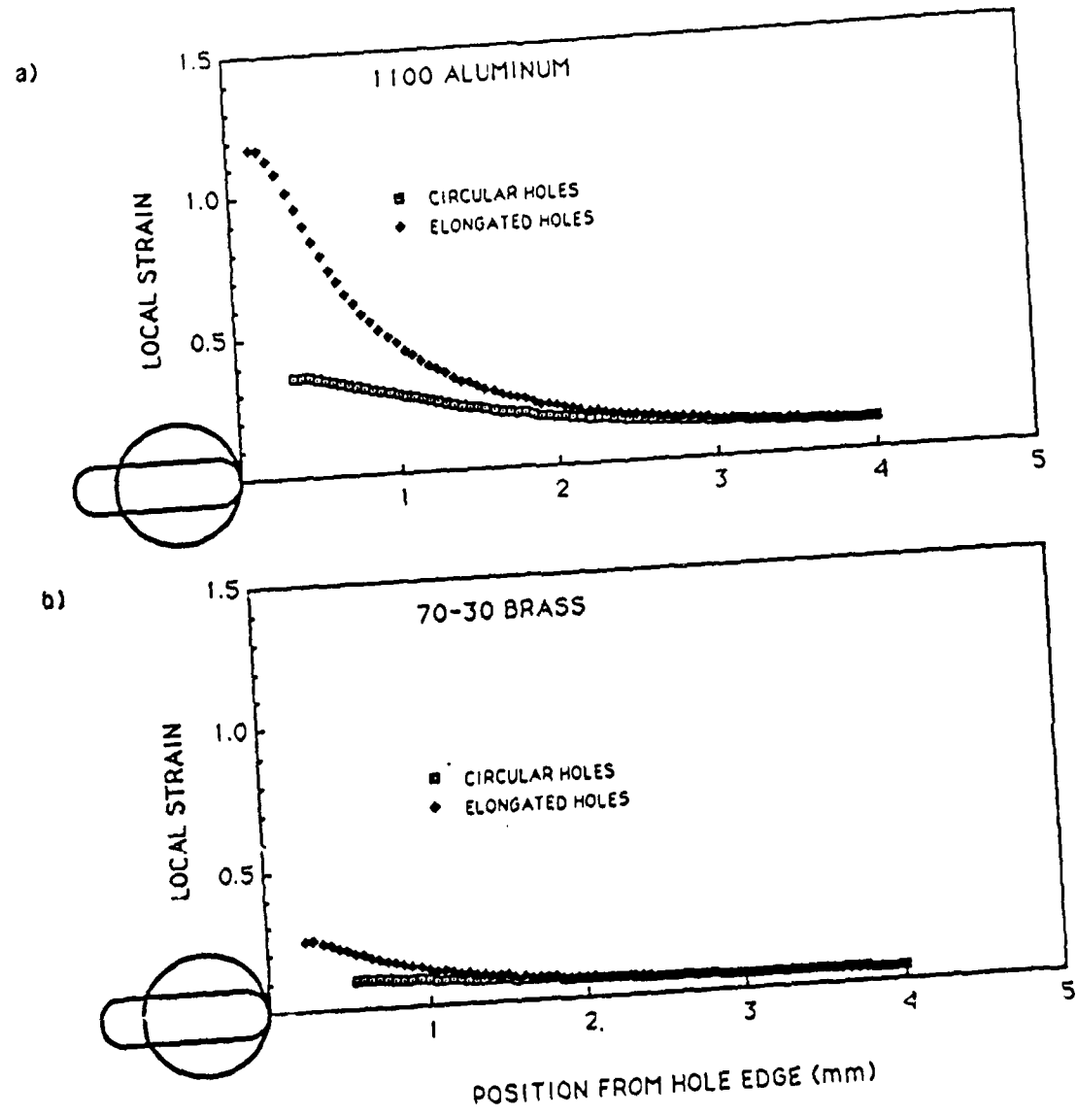

Figure 5. The predicted dependence of the local thickness strain component on position near circular or elongated holes in (a) '1100 Al' and (b) 'brass' and at macroscopic strain of 0.10. The strain profiles are along a line normal to the tensile axis passing through the center of the holes.

pore-induced crack initiation. Fig. 5 indicates that at distances greater than ~ 1 hole radius, the local strains are nearly equal for both circular and elongated holes. Thus for large interhole spacings, the element of ligament material midway between holes cannot recognize whether the holes are elongated or circular.

Current efforts are directed at establishing a more flexible, mechanics-base to the analysis by utilizing a Neuber analysis for describing plasticity near holes of ellipsoidal shape in materials with specified strain hardening rates [9]. This will extend the above analysis to a much wider range of hole/pore/void shapes and allow us to probe the role of strain hardening more rigorously. Collaborative research with Dr. Peter Matic of the Naval Research Laboratory is also planned to further extend our understanding of the linkage between microstructural geometry and local deformation and fracture processes. In particular, finite element calculations will be performed to describe local stress and strain distributions (and to verify the Neuber analysis) as well as to establish hole linking criteria in two dimensions and, ultimately, void linking criteria in three dimensions. Such an integrated approach is necessary to establish a valid computational model for predicting ductility given a general, three-dimensional void/pore microstructure in a material of known strain hardening.

(b) The Influence of Porosity on Low Cycle Fatigue of Metals

The principal results of this study have been described in the last Annual Report (10). Based on those results the following four manuscripts have been submitted for publication in the past year:

(1) "Porosity and Crack Initiation During Low Cycle Fatigue" (to be published in Materials Science and Engineering),

(2) "The Influence of Porosity on Short Fatigue Crack Growth at Large Strain Amplitudes (submitted to International Journal of Fatigue),

(3) "Cyclic Stress-Strain Behavior of Titanium in the Presence of Porosity" (accepted for publication in Modern Developments in Powder Metallurgy), and

(4) "On Modeling the Effect of Porosity on Crack Initiation During Low Cycle Fatigue", submitted to Int. J. of Powder Metallurgy.

2. PROCESSING AND PROPERTIES OF CU-NB ALLOYS (with Kevin Zeik, Ph.D. candidate and Dr. Iver Anderson, Ames Laboratory).

Processing alloys via rapid solidification has become a well established technique for obtaining alloys with for example, improved compositional uniformity, amorphous structures, or a supersaturation of an element which might be used to impart oxide dispersion strengthening. In the present study, rapid solidification is used in conjunction with high pressure gas atomization to impart novel microstructures which have the potential for excellent thermal stability and attractive mechanical properties. Although the present study utilizes Cu-Nb as a model system, the results should be applicable to other binary alloy systems whose equilibrium phase diagram is similar to that of Cu-Nb. Specifically, in such cases a nearly flat liquidus suggests the presence of a non-equilibrium liquid phase separation which under certain conditions can result in a high volume fraction of fine scale spheroidal multiphase particles. Such microstructures can be thermally stable to ~ 0.8 T_{MP} and may result in very attractive mechanical properties.

A key element in the present study is a phase diagram which exhibits a relatively flat liquidus extending over a broad range of compositions, such as in the Cu-Nb system; see Fig. 6. Such systems are known to be prone to metastable miscibility gaps and liquid phase separation [11-14]. The present study utilizes high pressure gas atomization (HPGA) and rapid solidification as a means of inducing liquid phase separation and novel fine-scale microstructures. As will be shown, the microstructural features which characterize the rapidly solidified powder particles are much different than a conventionally cast counterpart. The microstructural differences are such that they should result in significantly improved mechanical properties. The present study utilizes a Cu-21 w/o Nb alloy as a model system for demonstrating the above microstructural response.

Atomization of the Cu-21.2 w/o Nb alloy was performed at the Ames Laboratory, USDOE, where a new high pressure gas atomizer has been designed and constructed. This atomizer differs

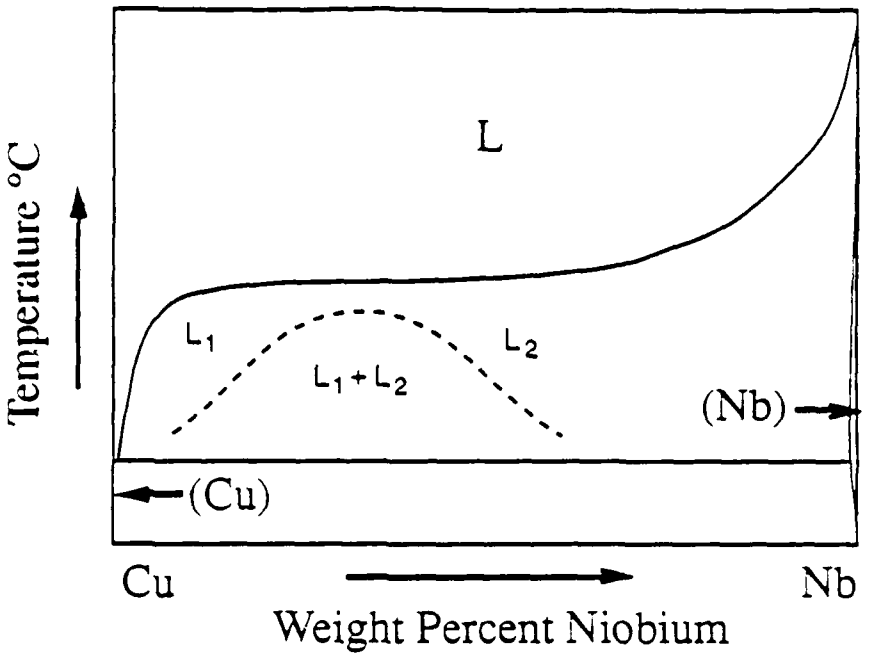

Figure 6. Schematic of the metastable miscibility gas (dashed lines) superimposed under the equilibrium phase diagram for the Cu-Nb alloy system.

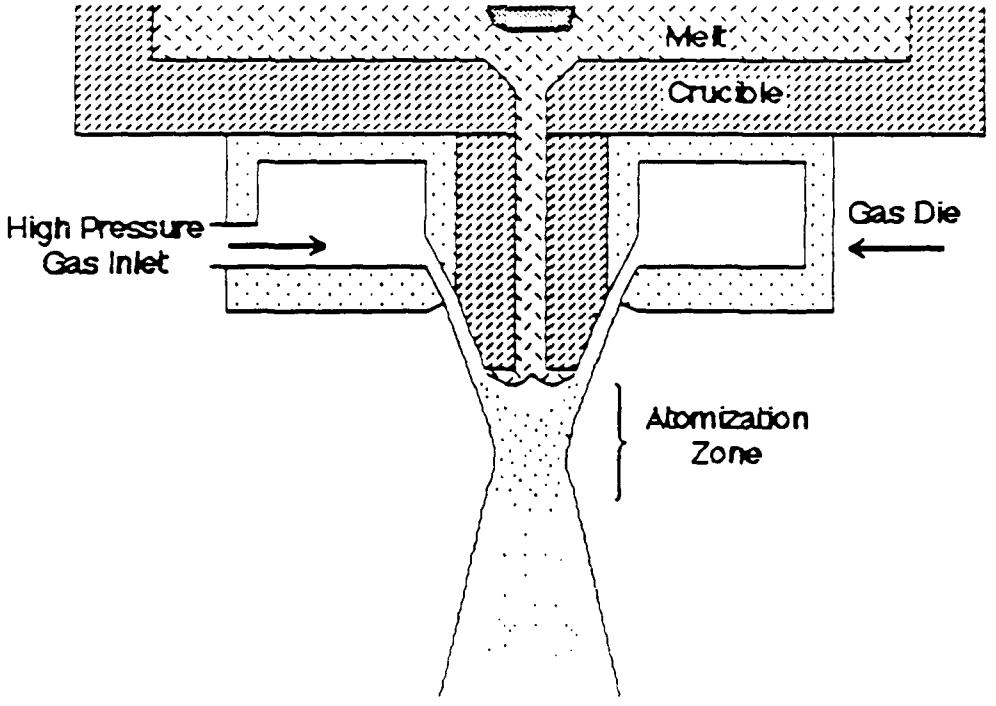

Figure 7. Schematic representation of the melt feed and nozzle configurations for the Ames Lab high pressure gas atomizer.

Figure 8. Scanning electron micrograph of the microstructure of a single, large (53μm) powder particle containing a distribution of niobium dendrites. The copper matrix has been chemically removed.

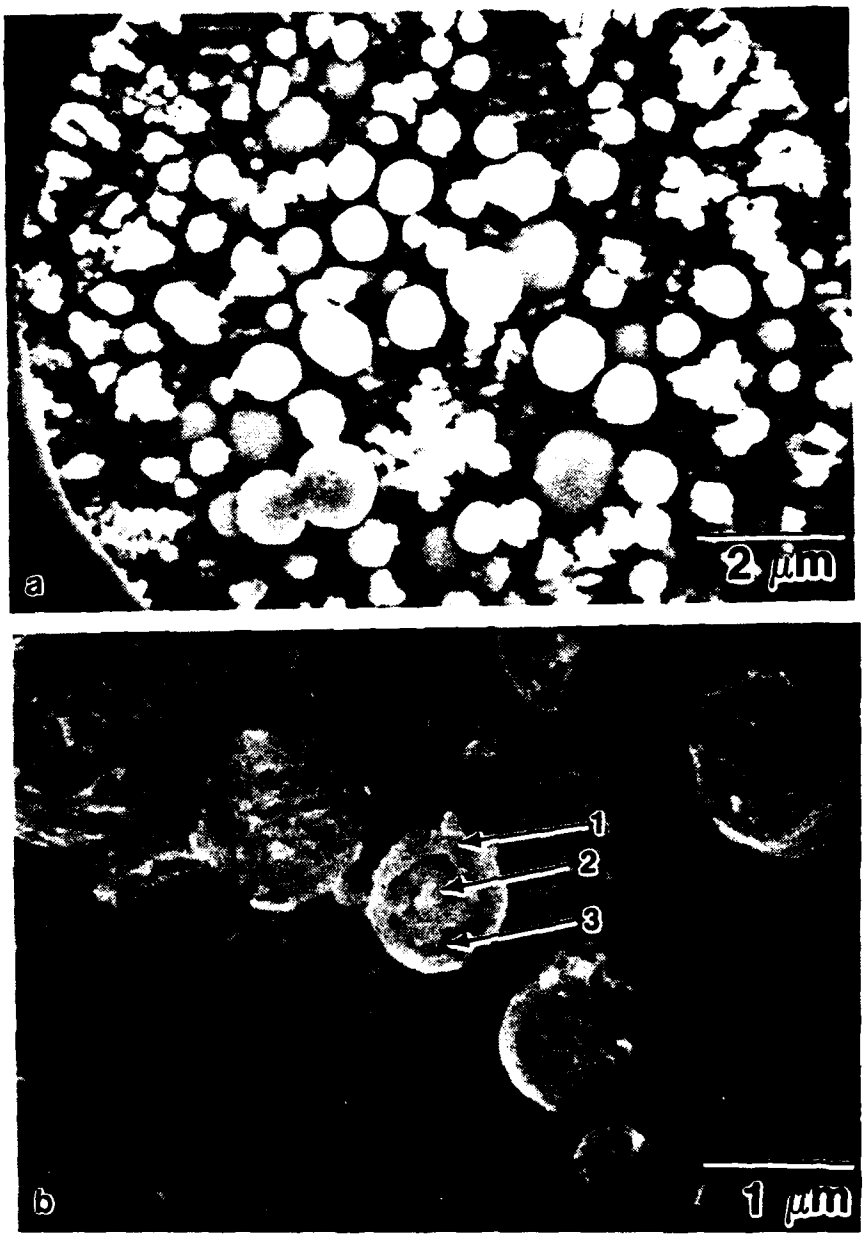

Figure 9. Scanning electron micrograph of a) the microstructure of a single, small (10μm) powder particle and b) a cross-section view of one single spheroid contained within this microstructure.

from other atomizers which are commercially used in that the melt delivery and nozzle configuration can produce a substantial yield of fine (<10μm) powders [15]. This process utilizes the high kinetic energy generated from the interaction of focused supersonic gas jets on a close-coupled melt stream to cause disintegration of the alloy into highly dispersed droplets of metal [16]; see Fig. 7. Given the fine-scale of the powders and large surface areas, special facilities were constructed to reduce the risk of powder contamination by using ultra high purity argon and a tornado-type separator to remove the powder from the atomization gas stream.

The microstructures generated during the HPGA of the Cu-Nb alloy depend on powder particle size. The "large" powder, classified herein as those particles between 45μm and 75μm in diameter, exhibited a microstructure which is typified by Fig. 8. The Nb-rich phase, the volume fraction of which was ≈22%, appeared as well formed, fine-scale dendrites (stalk diameters of 0.3 to 0.5μm) distributed within the Cu matrix. It should be noted that if all of the Nb present in a Cu-21.2wt%Nb alloy were present as a pure Nb second phase, then there would be 21.9 vol% second phase. The fact that the Nb-rich dendrites occupy ≈22% by volume is consistent with their being nearly pure Nb and agrees with observations of similar, slowly cooled Cu-Nb alloys [17].

In contrast to the above, the microstructures of the "fine" powders, classified as those less than 15μm in diameter, consist primarily of a distribution of spheroidal particles together with a few dendrites distributed within the copper matrix; see Fig. 9. Within the fine powder particles, the volume fraction of the Nb-rich phase measured ≈35% (10% dendrites + 25% spheres). This indicates that the spheroids are not pure Nb (assuming that the dendrites are nearly pure Nb). A cross-sectional view of the spheroids is shown in Fig. 9b and reveals that they are, in fact, multiphase. Backscatter SEM imaging in conjunction with EDS micro-analysis indicates that the spheroidal particles have Nb-rich shell, arrowed 1 in Fig. 9b, and an interior consisting of both Nb- and Cu-rich phases, arrowed 2 and 3, respectively. The significant amounts of Cu in the spheroidal particles results in the enhancement of the "second" phase volume fraction from ≈22% in the large powder particles to ≈35% in the fine particles. The diameter of the spheroid particles

within the fine powders varied from <0.1 to 2.0μm. In addition, a few small dendrites were observed at both the particle surface and randomly distributed within the interior.

Given the small volumes of the fine powder particles, the above observations suggest that a high degree of undercooling occurs in the fine (<15μm) powder droplets either prior to or during the very early stages of their solidification. Such behavior is consistent with previous data in which fine (<10μm) droplets of both Cu-Si and Cu-Al alloys exhibited large undercoolings to $0.23T_m$ and $0.28T_m$, respectively, prior to solidification. It thus is reasonable to conclude that the resulting undercooling of the fine powders provide access to the metastable liquid miscibility gap, promoting liquid phase separation and resulting in a dispersed, spherical phase in a continuous matrix. A schematic of the metastable miscibility gap is also given in Figure 6.

The fine and medium scale powder particles both contain spheroids as well as dendrites, as shown in Fig. 10 suggesting that the microstructural evolution in this Cu-Nb alloy depends not only upon the degree of undercooling prior to solidification but also on cooling rate, which depends on particle size. Specifically, the cooling rate appears to influence the degree of undercooling attained by each droplet prior to solidification, hypothesized as establishing a kinetic competition between liquid phase separation and Nb dendrite formation. A key observation is that the fine (<15μm) powders, capable of both the largest amount of undercooling and fastest cooling rate, exhibit microstructures consisting of primarily Nb-rich multiphase spheroids dispersed within a Cu matrix, whereas larger particles contain an increasing amount of dendrites, until finally a size is reached when Nb dendrites dominate the microstructure of the powder particles.

The above results suggest a solidification path, schematically presented in Fig. 11, by which the solidification process depends on a metastable phase separation of the liquid, as presented in the phase diagram, Fig 6. At $t_0=0$, atomization of the melt into various size droplets of the Cu-21.2wt%Nb liquid occurs. At $t_1>t_0$, the smallest droplets (<15μm) which are likely to be free of hetereogeneous nucleation sites, undercool to a degree that Nb-rich liquid separates into small spherical pools throughout a Cu-rich liquid matrix. This occurs by either nucleation and growth

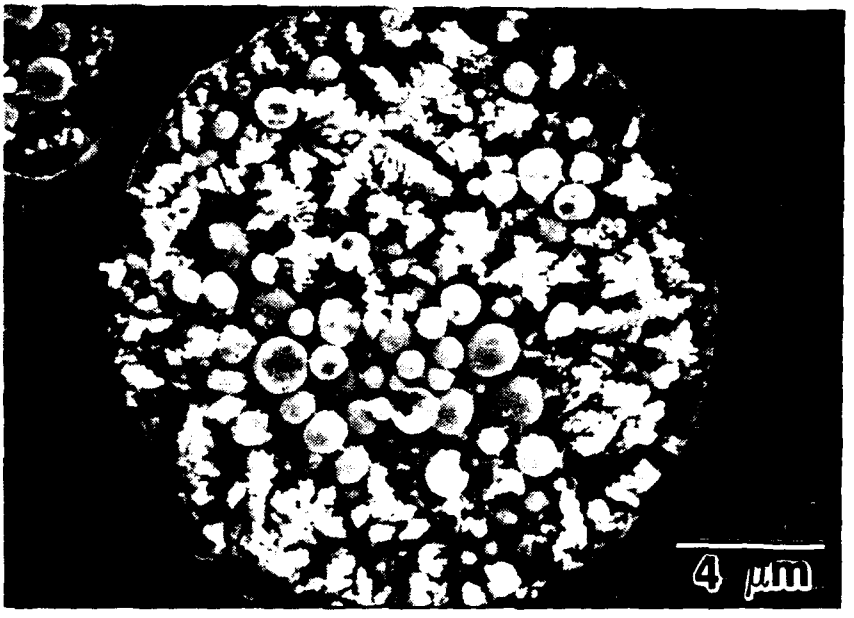

Figure 10. Scanning electron micrograph of the microstructure of a medium (20μm) size powder particle which contains large amounts of both niobiuim-rich spheroids and dendrites.

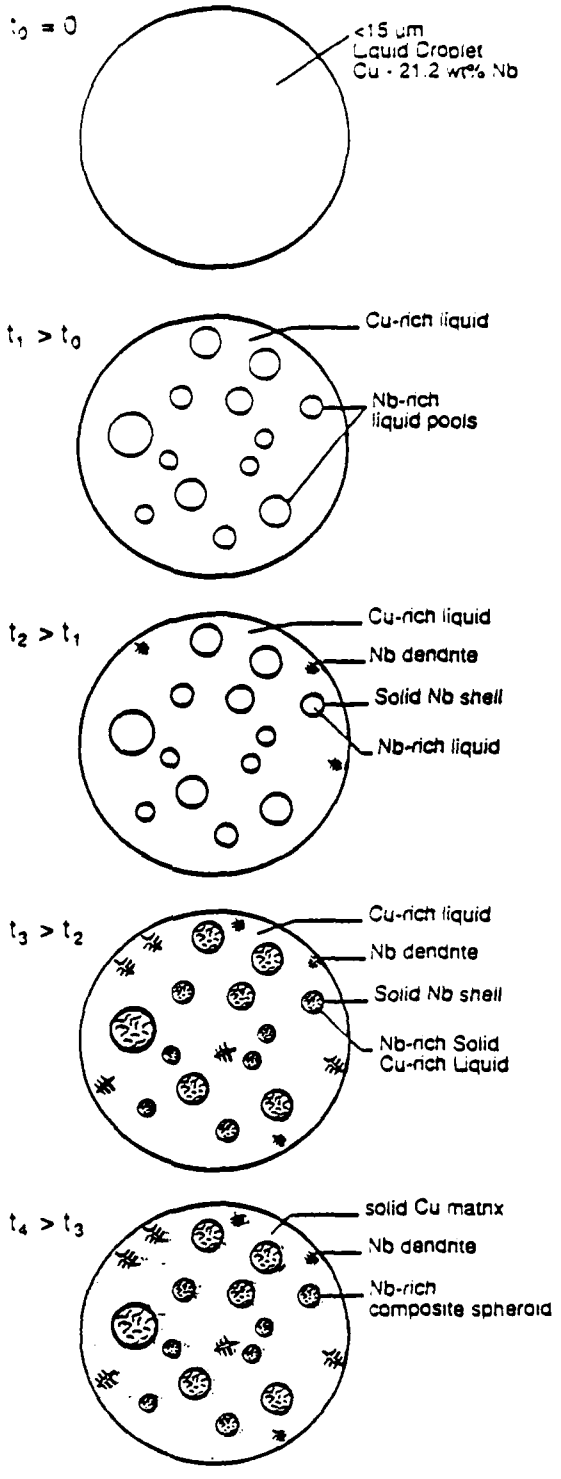

Figure 11. Schematic representation of the solidification path experienced by a small (<15μm) Cu-Nb droplet formed during atomization.

and/or by spinodal decomposition [19]. We estimate that at temperatures near solidification, the Nb-rich liquid has a compositions of roughly Cu-50wt%Nb.*

At some point, schematically represented as $t_2>t_1$ on Fig. 11, heterogeneous nucleation of solid Nb at a liquid/liquid interface within the fine droplets commences, as the large amount of undercooling achieved by the droplet overcomes the activation barrier to form solid Nb. The spherical nature of this dispersion suggests that it had formed before the matrix had solidified while its fine scale suggests that the cooling rate had been effective in preventing coalesence. In addition, we suggest that the rapid cooling rates promote further undercooling by limiting the extent of growth of any solid niobium which may have nucleated and grew dendritically [19].

At $t_3>t_2$, recalesence, in addition to the isolation effect of the continuous shell, causes the interior of the Nb-rich "spheroids" to slowly solidify along an equlibrium path. This results in the multiphase nature of the spherical particles; as shown in Fig. 7b. In addition, the latent heat generated by the formation and subsequent solidification of the Nb-rich spheroids slows the cooling rate of the Cu-rich liquid matrix and allows it to also begin to solidify along an equilibrium path. A few, small niobium dendrites will thus nucleate and grow as the copper-rich liquid follows the equilibrium liquidus, rejecting solute as the temperature decreases. At $t_4>t_3$, the final solidification event occurs as the nearly pure Cu matrix solidifies around both the spheroidal and dendritic particles.

Given their size, the large (45 - 75μm) powder particles are expected to contain potent heterogeneous nucleation sites (motes) and to cool at a rate such that the solidification path conforms to that predicted by the equilibrium phase diagram, Figure 6. Upon atomization, these droplets are not likely to undercool to the extent required to cause liquid immiscibility, since there exists a high probability that each would contain effective heterogeneous nucleation sites. This would prevent access to the liquid phase separation and promote nucleation and growth of solid Nb, forming a fine dispersion of dendrites within a Cu matrix, the size and distribution of which is related to the cooling rate of that particle.

---

* This is based on the assumption that the Nb-rich dendrites are pure Nb and that 35 vol% of (spheres + dendrites) is achieved by spheres of composition Cu-50 wt% Nb in this Cu-21.2 wt% Nb alloy.

The benefit of the microstructural manipulation via high pressure gas atomization in systems such as Cu-Nb is the possibility that such fine-scale, "microcomposite" microstructures will impart superior properties. Current efforts are focusing on the stress-strain behavior of bulk specimens which have been HIP consolidated from powders of different size and therefore exhibiting different microstructures. As shown in Fig. 12 preliminary results indicate that stress-strain response of bulk specimens is a function of prior powder particle size with "medium-sized" powder material possessing a higher flow stress. Both tensile and compressive tests are currently being conducted to determine stress-strain behavior from -196°C to 600°C of bulk specimens processed from a range of powder particle sizes. The thermal stability of the alloy microstructures is also being investigated for conditions up to 900°C/100 hrs. Microstructural analysis utilizing TEM is also underway; thin foil specimens for TEM examinations are being prepared using a combination of electrolytic twinning and ion beam milling.

3. A NEW AGE-HARDENABLE BETA TITANIUM SYSTEM (with Lou Quattrocchi, M. S. candidate)

Age hardenable beta (bcc) Ti alloys usually rely on the formation of alpha-phase (hcp) precipitate particles for their high strength, and as such, are limited to use temperatures of about 400°C. This is unfortunate since beta Ti alloys are known to be more cold formable, more resistant to hydrogen embrittlement, and in some instances, exhibit much higher yield strengths and fracture toughnesses than their alpha-beta counterparts. Given the amount of refractory elements (V, Nb, etc) present as beta-phase stabilizers in beta Ti alloys, it is also likely that they are less burnable than the alpha-phase alloys. This would make them attractive for high temperature gas turbine applications where a susceptibility to burning has limited Ti alloy usage in the compressor section. The purpose of the present research is to explore the use of precipitates based on the orthorhombic phase (O-phase) to age harden a beta-phase Ti-Nb-Al alloy. As will be demonstrated, the alloy Ti-23 Nb-11 Al (in at%) exhibits a strong age hardening response in a temperature range 600°C, which is about 100°C higher

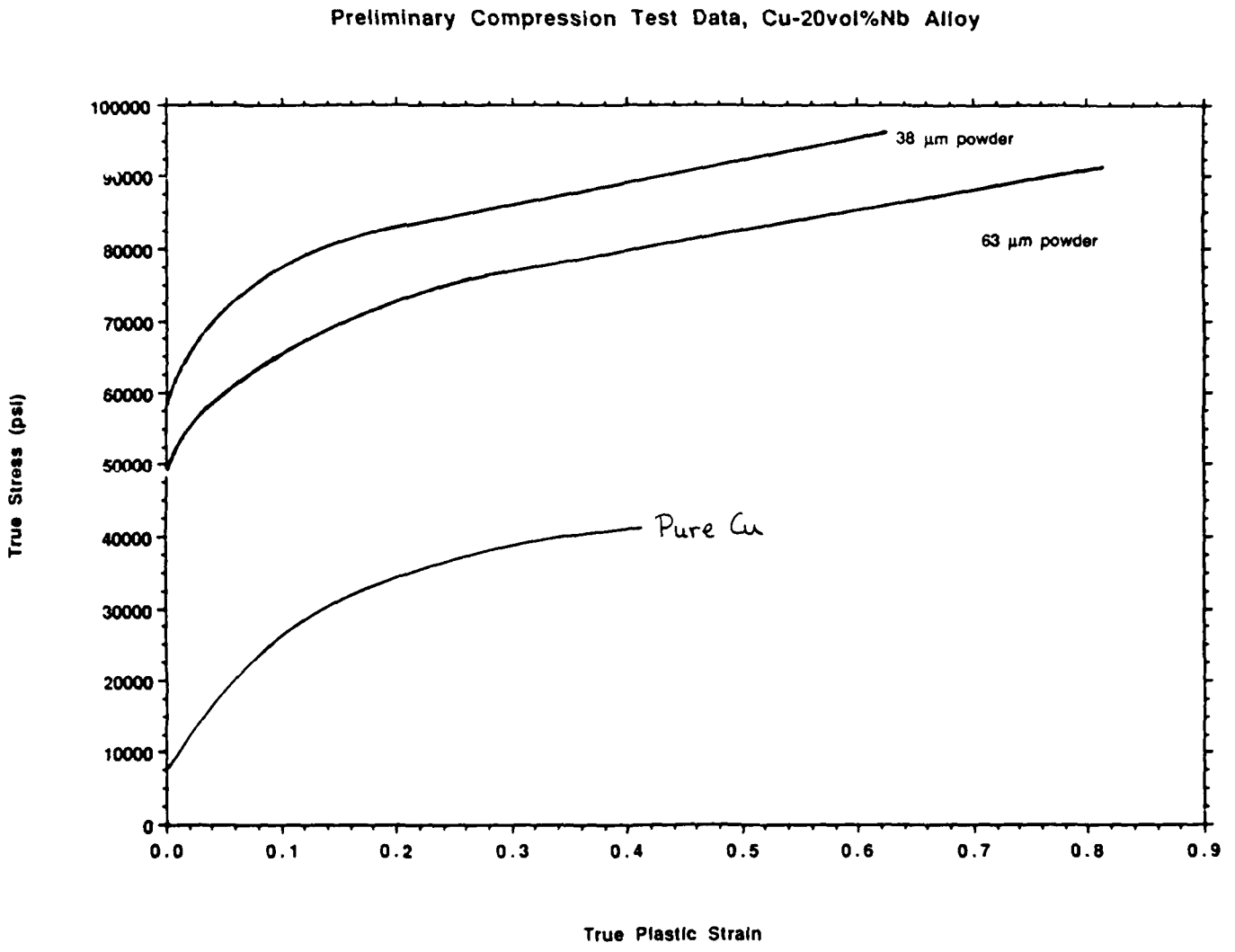

Figure 12. Compressive stress-strain responses of pure Cu as compared to bulk specimens consolidated from "large" powder (63μm average particle size) and "medium" powder (38μm average size).

than that used to age harden conventional beta Ti alloys. This implies the possibility of significantly higher use temperatures of this type at beta Ti alloy.

The basis for the present alloy system is the observation by Banerjee and co-workers that in Ti_3Al alloys containing large amounts of Nb ($\geq$ 11 at. %), an ordered orthorhombic phase, the "O-phase", can form [20]. Its composition is based on Ti_2 Al Nb. Further research by Gittis and Koss on Ti-23Nb-11Al (whose composition corresponds to the beta phase in the Ti_3Al-based alloy Ti-24Al-11Nb) indicated that O-phase precipitates form in as-quenched specimens aged at 760°C for two hours [21]. This research program extends those observations by examining the age hardening response of the Ti-23Nb-11Al alloy.

Fig. 13 shows the age hardening response of the Ti-23Nb-11Al alloy at 575°C and 625°C. In both cases, the alloy was He-gas quenched from 1000°C, since our data indicate a solvus temperature for the age-hardening phase of about 980°C. As is evident from Fig. 13, a large increase in hardness occurs at both 575 and 625°C. Overaging occurs at 625°C but at 575°C there is only a small ($\simeq$ 15DPH) decrease in hardness after 48 hrs aging. Separate experiments indicate that cold work in the form of 10% and 30% reduction in thickness had no significant effect on the age hardening response at 575°C.

Currently, both tensile and compression specimens have been prepared and will be tested in the solution-treated and aged conditions over a range of temperatures up to 550°C. In addition, TEM specimens are being prepared for phase identification; this research will be performed in cooperation with G. Scarr at GE Aircraft Engines, Cincinnati. The combined results of the mechanical tests and the associated electron microscopy should establish the mechanism of strengthening in this novel age-hardenable beta Ti alloy system. Any development of a new family of age-hardenable beta Ti alloys strengthened by precipitates based on the O-phase will clearly utilize the pioneering results of this study.

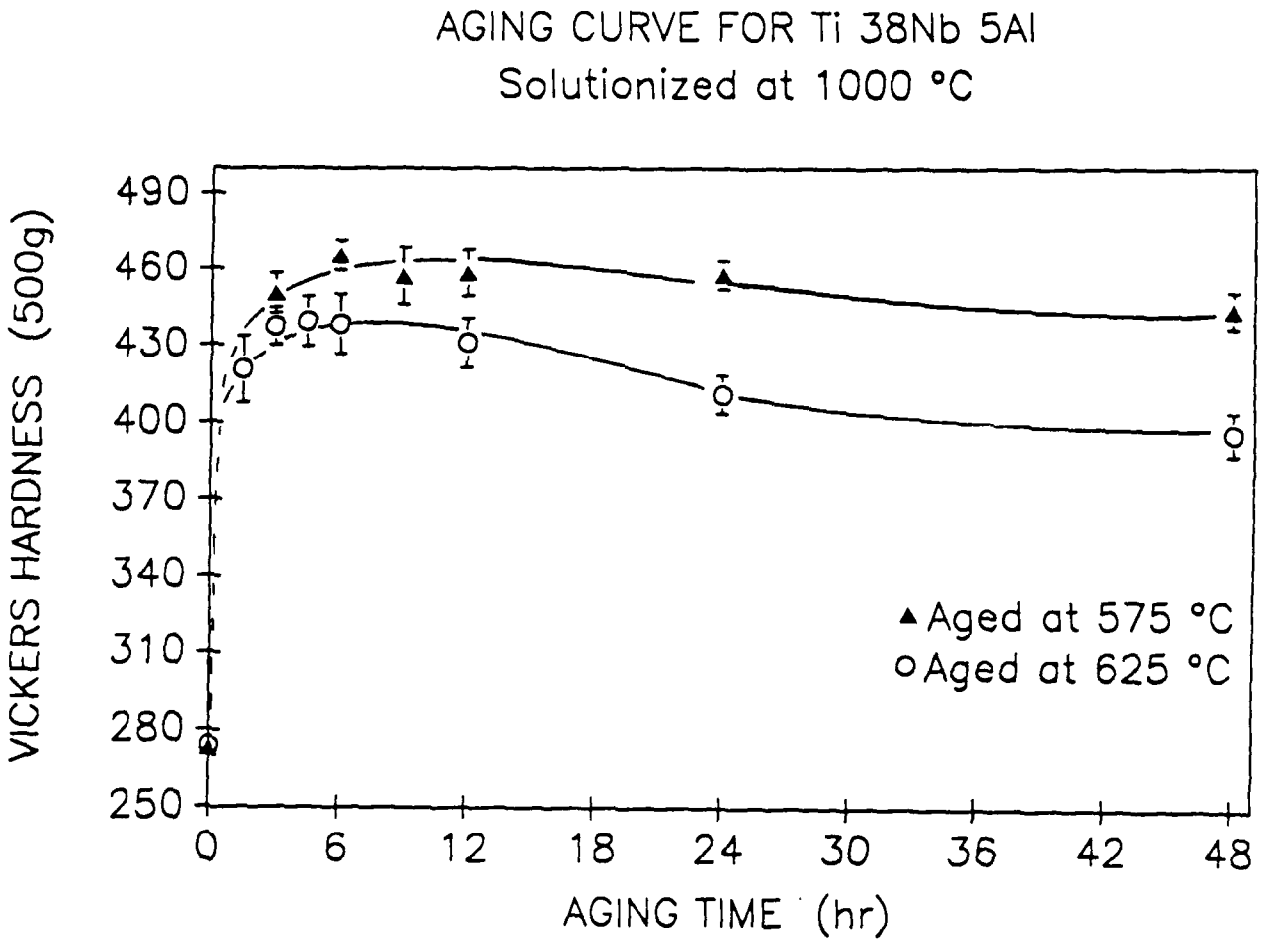

Figure 13. The age hardening response of Ti-38Nb-5Al quenched from 1000°C and aged at either 575° or 625°C.

REFERENCES

1. R. Haynes, the Mechanical Behavior of Sintered Alloys, Freund Publishing House, London, 1981.

2. K. M. Vedula and R. W. Heckel, Modern Deve. in Powder Met. Vol. 12 (ed H. H. Hausner, H. W. Antes, and G. D. Smith) MPIF, Princeton, 1981, p. 759.

3. T. J. Griffiths, R. Davies, and M. B. Bassett, Powder Metall. 22, 119 (1979).

4. P. E. Magnusen, D. A. Koss, E. M. Dubensky, Acta Metall. 36, 1503 (1988).

5. E. M. Dubensky and D. A. Koss, Metall. Trans. A 18A, 1887 (1987).

6. P. E. Magnusen, D. J. Srolovitz, and D. A. Koss, Acta Metall. (in print).

7. A. Geltmacher and D. A. Koss, Int. J. Powder Met. (in print).

8. A. Geltmacher and D. A. Koss, Technical Report No. 14, ONR Contract No. N00014-86-K-0381, April 1990.

9. H. Neuber, Trans. ASME 28 544 (1961).

10. D. A. Koss, Technical Report No. 10 ONR Contract No. N00014-86-K-0381, April 1989.

11. J. D. Verhoeven and E. D. Gibson, J. Mat. Sci., 13 1576 (1978).

12. S. P. Elder, A. Munitz, and G. J. Abbaschian, Mat. Eng. Forum, 50 137 (1989).

13. S. K. Dhua, S. Raju, and K. Chattopadhyay, Met. Trans. A, 18A 1131, (1987).

14. J. H. Perepezko and W. J. boettinger, MRS Symp. on Alloy Phase Diagrams, L. H. Bennett, T. B. Massalski, and B. C. Giessen eds., Vol. 19, p. 223. Elsevier, North-Holland (1983).

15. I. E. Anderson and B. B. Rath, in Rapidly Solidified Crystalline Alloys, S. K. Das, B. H. Kear, and C. M. Adam eds., p. 219, The Metallurgical Society of AIME, Warrendale, PA (1985).

16. I. E. Anderson and R. S. Figliola, in Modern Developments in Powder Metallurgy, Vol. 20, p. 205 (1988).

17. K. L. Zeik and I. E. Anderson, Unpublished Work.

18. I. E. Anderson and M. P. Kemppainen, in Undercooled Alloy Phases, E. W. Collings and C. C. Koch eds., The Metallurgical Society of AIME, Warrendale, PA, (1986).

19. J. H. Perepezko, Alloy Phase Diagrams K. H. Bennett, J. B. Massalaski, and B. C. Giessen eds., (Mat. Res. Soc.) 1983 p. 223.

20. D. Banerjee, A. K. Gogia, T. K. Nundy, and V. A. Joshi, Acta Met. 36 871 (1988).

21. S. J. Gittis and D. A. Koss in High-Temperature Ordered Intermetallic Alloys III, C. T. Liu, et al eds. (Mat. Res. Soc.) 1989 p. 323.